BNL-211211-2019-TECH

NSLSII-ASD-TN-276

Concept of the Complex Bend

T. Shaftan

January 2018

Photon Sciences

Brookhaven National Laboratory

U.S. Department of Energy

USDOE Office of Science (SC), Basic Energy Sciences (BES) (SC-22)

DISCLAIMER

NSLS II TECHNICAL NOTE BROOKHAVEN NATIONAL LABORATORY	NUMBER NSLSII-ASD-TN-276
AUTHOR T. Shaftan, V. Smaluk and G. Wang	DATE 1/25/2018
TITLE Concept of the Complex Bend	

Abstract

Modern synchrotron lattices follow Multi-Bend Achromat approach [1] and realize low emittance by arranging small horizontal beta-function and dispersion in the bends. In this paper we propose another optics solution aimed to reach low emittance by using a lattice element that we named as “Complex Bend”. The Complex Bend corresponds to a strong alternate focusing distributed along the bend so to maintain the beta-function and dispersion oscillating at low values. Comprising the ring lattice out of Complex Bends instead of regular dipoles will minimize the $\mathcal{H}$-function and reduce the horizontal emittance while localizing bending to a small fraction of the storage ring circumference. The latter should help to gain more space for Insertion Devices.

In the following, we present the concept of Complex Bend, considerations on the choice of its optimal parameters, as well as, thoughts of its practical realization. This paper gives a snapshot where our current studies stand and does not pretend to be a complete description of the Complex Bend engineering design and integration of this element into a specific ring lattice.

1. Comparison between the regular dipole and the Complex Bend

The trend of minimizing emittance of modern storage rings translates into reduction of dispersion and beta-functions in their lattice dipoles. Majority of the recent facility upgrades [2-5] are based on employing MBA lattices, i.e. introducing a number of short bending dipoles with strong focusing quadrupoles in between, which aids in maintaining lattice functions at smaller values as compared with conventional DBA or TBA lattice solutions. The number of MBA cells per machine superperiod vary between 5 (MAX-4) to 19 (MAX-4 upgrade) for the latest designs [6].

It is customary to relate the ring emittance with the number of dipoles in the ring as $\varepsilon_x = F(\nu_x, lattice)\frac{E^2}{J_x N_d^3}$, where E is the beam energy, J_x is horizontal partition number and N_d is the number of dipoles in the ring. We propose to substantially decrease the beam emittance by increasing the number of magnets and combining them into a single element as poles with the same field polarity separated by strong quadrupoles of the alternative polarity. To illustrate our approach we recall that APS contains 40 x 2 = 80 dipoles and APS-U is based on 40 x 7 = 280 dipoles. In the concept below we will be considering 1200 bends treated as separate poles of the several complex structures.

The concept of the element, a.k.a. Complex Bend, is in the following (Fig. 1).

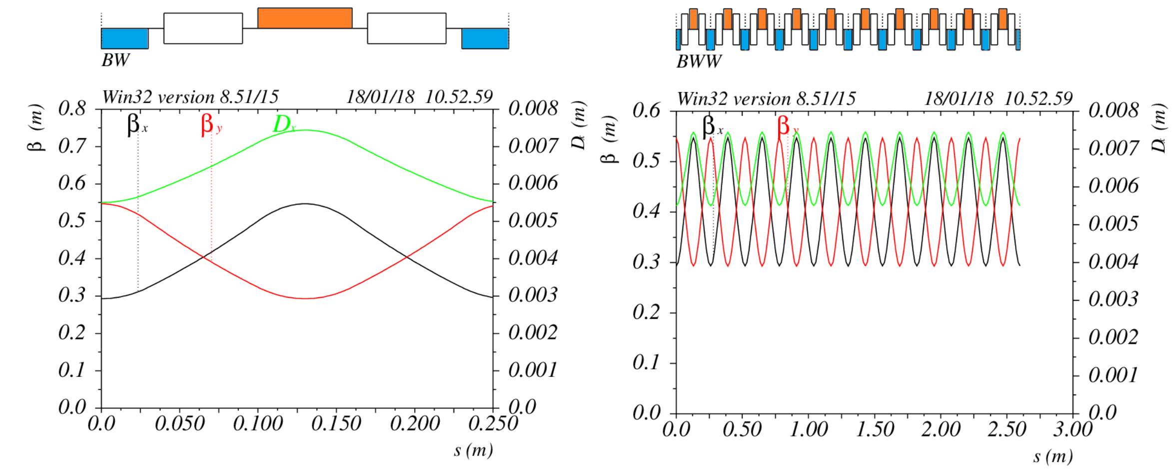

Fig. 1: Left figure shows a single cell of Complex Bend. The cell consists of two quadrupoles separated by short dipoles. Right figure shows an assembly of N cells representing a complete Complex Bend.

The element provides with distributed focusing and bending of the particle beam (Fig. 1). A single cell is featured by the cell advance that depends on a combination of quadrupole gradients in quadrupole and field in the dipole magnets, their length and the distance between the consecutive poles.

Short periods of Complex Bend (~10 cm) are of practical interest and, as easy to estimate, they result in high gradients of the pole fields. In Fig. 2 we present a comparison between NSLS-II bending dipole, Theoretical Minimum Emittance conditions for the same case and Complex Bend corresponding to the same magnet bending angle (6°) and length. For this particular example we have chosen K_{1F}=100 m^{-2} and K_{1D}=-80 m^{-2}, which gives us additional horizontal focusing helping to reduce horizontal beta-function and dispersion lowering $\mathcal{H}$-function by factor 2 at the expense of somewhat higher vertical beta-function.

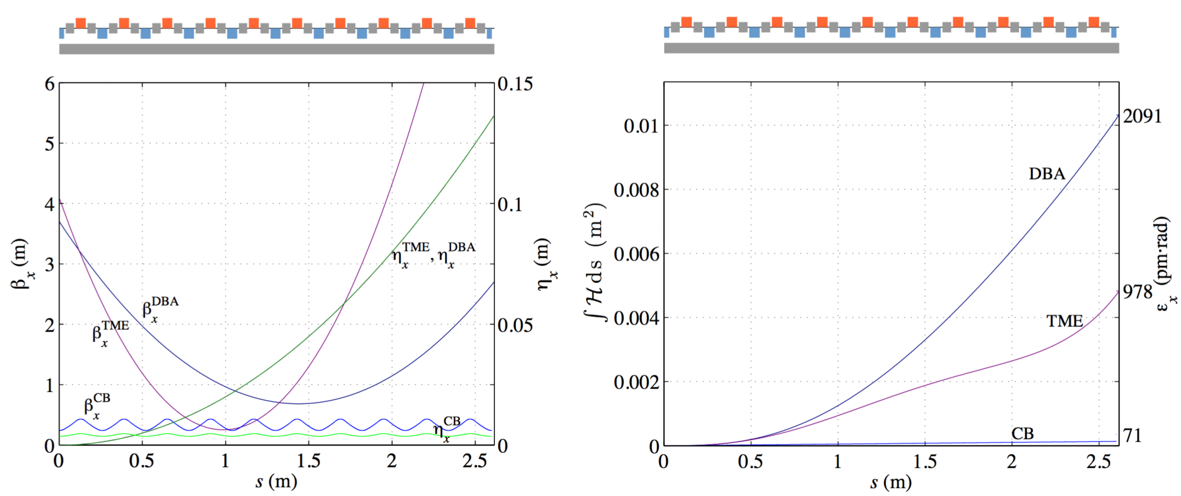

Fig. 2: Comparison between NSLS-II bending dipole, TME and Complex Bend. The left plot shows beta-function and dispersion, and the right plot presents with integral of $\mathcal{H}$-function from 0 to s for the three cases. The corresponding emittance values are shown on the right scale of the right plot.

As follows from the plots the Complex Bend results in smaller beta-functions and dispersion, thus, resulting in a smaller integral of $\mathcal{H}$-function (Fig. 2, right). Table 1 lists parameters of the NSLS-II bending dipole against that for the Complex Bend that we used in our calculations.

	NSLS-II dipole	Complex Bend
Length, m	2.6	2.6
Bending field, T	0.4	1.05
Period length, L_{CB}, cm	-	26
Bending angle, rad	0.105	0.105
K_1, m^{-2}	0	+100/-80
βx_{max} / βx_{min}, m	3.7 / 0.7	0.42 / 0.24
η_{max} / η_{min}, mm	137 / 0	4.72 / 3.58

Table 1: Parameters of NSLS-II dipole and Complex Bend used in the calculation.

As follows from Table 1 the required range of K_1 gradients is at the level of 100 m^{-2} or higher. Indeed a combination of K_1 and pole length values as taken above gives the focusing distance of individual quadrupoles in the lattice of Complex Bend of 20 cm. For the range below 100 m^{-2} the gain of the Complex Bend over conventional magnets rapidly diminishes as will be evident from the analysis in the next section. For the beam energy of 3 GeV this translates into the requirement of quadrupole gradient in the range of 500-1000 T/m.

Advantage of the Complex Bend over the conventional dipole is increasing with the length of the former due to the natural divergence of lattice function with distance in the latter. For a long Complex Bend, the radiation emitted in Complex Bend field will impinge on the inner walls of the aperture, thus, provisions need to be made to extract the radiation from inside of the element.

Lastly, we approximated the Twiss functions and dispersion for a FODO cell of Complex Bend of length L_{CB} with expressions like $A(s) \approx A_0 + \Delta A \cdot cos\left(2\pi \cdot \frac{s}{L_{CB}}\right)$, which are quite accurate for the relatively small phase advances that we consider in our cases of interest. These expressions help to find synchrotron integrals for a given ring lattice and obtain analytic dependencies of $\mathcal{H}$-function on the dipole and quadrupole fields.

We worked out analytic expressions for the case when K_{1F}=K_{1D}. Below we used the following notation:

μ_d=$k_0 \cdot L_d$, μ_q=$K_1^{0.5} \cdot L_q$ are the betatron phase advances through the dipole and quadrupole poles correspondingly (K stands for scaled element strength).

$$C_h = cosh(\mu_q), S_h = sinh(\mu_q), C_n = cos(\mu_q), S_n = sin(\mu_q), C_d = cos(\mu_d), S_d = sin(\mu_d),$$

$$C_{0.5h} = cosh\left(\frac{\mu_q}{2}\right), S_{0.5h} = sinh\left(\frac{\mu_q}{2}\right), C_{0.5n} = cos\left(\frac{\mu_q}{2}\right), S_{0.5n} = sin\left(\frac{\mu_q}{2}\right), L_D = 2L_{dr} + L_d$$

Betatron phase advance through a cell of the Complex Bend is:

$$cos(\mu_{CB}) \approx C_n C_h - 0.5{L_D}^2 K_1 S_n S_h + L_D K_1^{0.5}(C_n S_h - C_h S_n)$$

We neglected focusing from the dipole poles in the expression above. Maximum and minimum of β_x are given by the expression below:

$$\begin{pmatrix}\beta_{xmin}\\ \beta_{xmax}\end{pmatrix} \approx \frac{1}{K_1^{0.5}\sin(\mu_{CB})}\begin{pmatrix} S_n + C_n S_h - L_D K_1^{0.5}\left(S_n S_h - 2C_{0.5h}^2 C_n\right) - L_D^2 K_1 C_{0.5h}^2 S_n \\ S_h + C_h S_n + L_D K_1^{0.5}(S_n S_h + C_n C_h + C_h) + \frac{1}{2} L_D^2 K_1 C_h (1 + C_n)\end{pmatrix}$$

and dispersion is expressed in the following form:

$$\begin{pmatrix}M_{13} + M_{13}^*\\ M_{13} - M_{13}^*\end{pmatrix} = \begin{bmatrix}2 - (M_{11} + M_{11}^*) & M_{11} - M_{11}^* \\ M_{11}^* - M_{11} & 2 + (M_{11} + M_{11}^*)\end{bmatrix}\begin{pmatrix}\eta_{xmin}\\ \eta_{xmax}\end{pmatrix},$$

where

$$\begin{gathered}
M_{11}^* = C_{0.5\mathrm{n}} C_1^* - K_1^{0.5} S_{0.5\mathrm{n}}\left(C_d\left(L_{dr} C_{0.5h} + S_{0.5h} K_1^{-0.5}\right) + L_{dr} C_1^* + C_{0.5h} S_d k_0^{-1}\right) \\
M_{11} = C_{0.5h} C_1 + K_1^{0.5} S_{0.5h}\left(C_d\left(L_{dr} C_{0.5n} + S_{0.5n} K_1^{-0.5}\right) + L_{dr} C_1 + C_{0.5n} S_d k_0^{-1}\right) \\
M_{13}^* = S_{\mathrm{d}} K_1^{-0.5}\left(S_{0.5h} + K_1^{0.5} L_{dr} C_{0.5h}\right) - C_{0.5h}(C_d - 1) k_0^{-1} \\
M_{13} = S_{\mathrm{d}} K_1^{-0.5}\left(S_{0.5n} + K_1^{0.5} L_{dr} C_{0.5n}\right) - C_{0.5n}(C_d - 1) k_0^{-1} \\
C_1^* = C_{\mathrm{d}} C_{0.5\mathrm{h}} - k_0 S_d\left(L_{dr} C_{0.5h} + S_{0.5h} K_1^{-0.5}\right) \\
C_1 = C_{\mathrm{d}} C_{0.5\mathrm{n}} - k_0 S_d\left(L_{dr} C_{0.5\mathrm{n}} + S_{0.5h} K_1^{-0.5}\right)
\end{gathered}$$

The following figure illustrates a comparison between approximate analytic expressions above with the result from matrix multiplication.

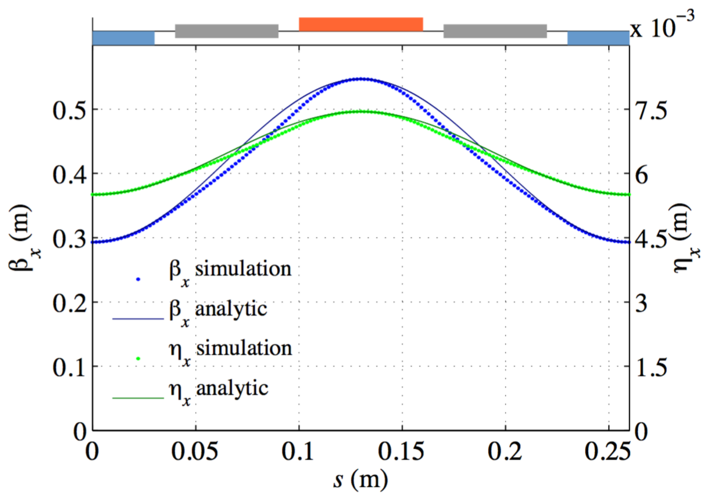

Fig. 3: Analytic expressions (dots) versus simulation results along a single cell for $\beta_x$and η_x.

Using these expressions we calculate the ring emittance with the Complex Bends as:

$$\varepsilon_x \approx C_q \gamma^2 \frac{\eta_d^2}{R_d \beta_{xd}},$$

Where the subscript "*d*" marks the average parameters $(\beta_{xmax} + \beta_{xmin})/2$, $(\eta_{xmax} + \eta_{xmin})/2$ in the dipole.

2. Magnet lattice and Twiss parameters

In this section we explore the range of parameters for the Complex Bend and discuss its scaling with field values and gradients. In the following we selected four betatron phase advances per cell of the Complex Bend (0.06, 0.08, 0.11, 0.14). We used transport matrices and expressions presented in Section 1 to compute periodic lattice solutions and extract lattice functions, emittance and chromaticity.

First we studied scaling of required K_1 with respect to the length of the cell $2\cdot (L_q+ L_D + 2\cdot L_d)$. We conclude (Fig. 4) that the maximum technically achievable gradient limits the minimum length of the cell thus controlling the total length of the device. Twiss functions and dispersion maxima, together with $\mathcal{H}$-function monotonically reduce as a function of scaled quadrupole gradient. Lower values of the $\mathcal{H}$-function and, hence, machine emittance require large phase advance per cell and high values of K_1.

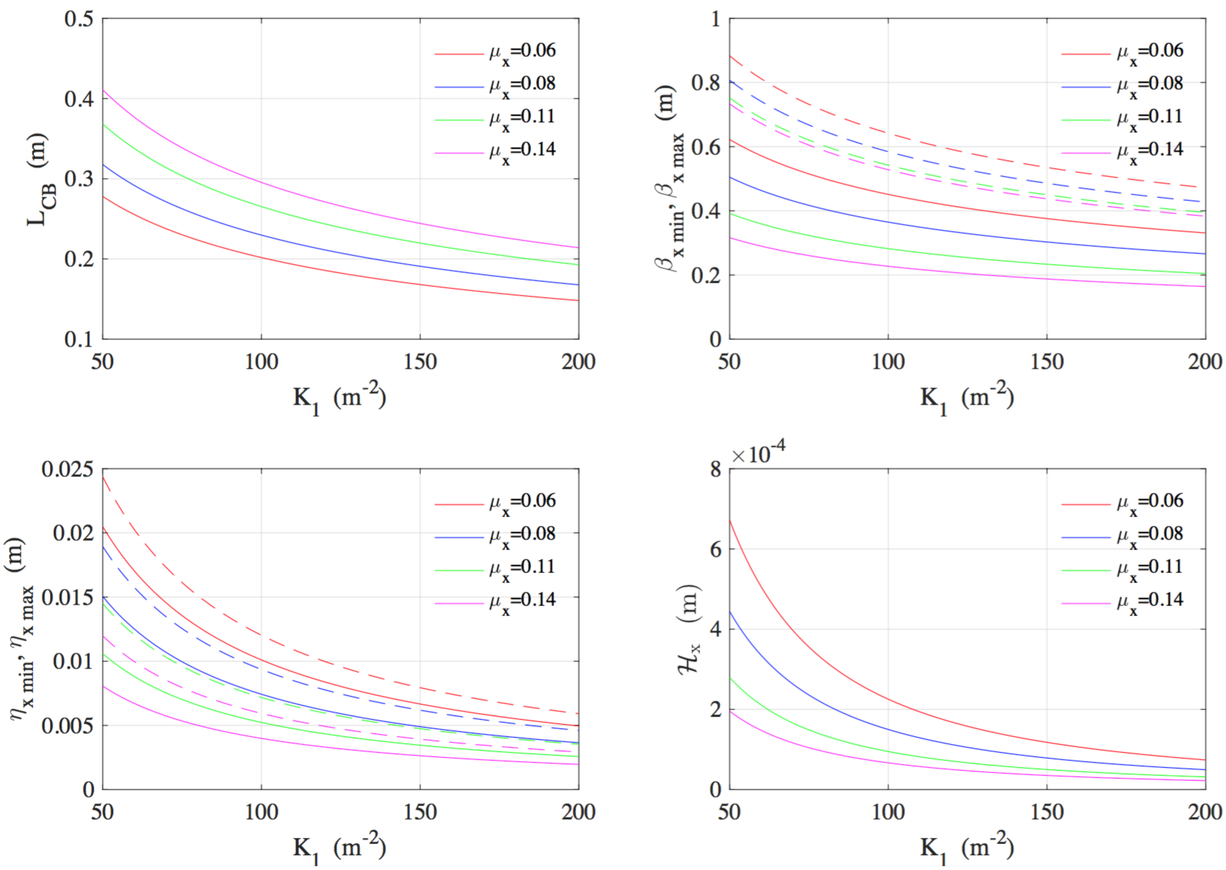

Fig. 4: Scaling of Complex Bend 's parameters including beta functions, dispersion and $\mathcal{H}$-function

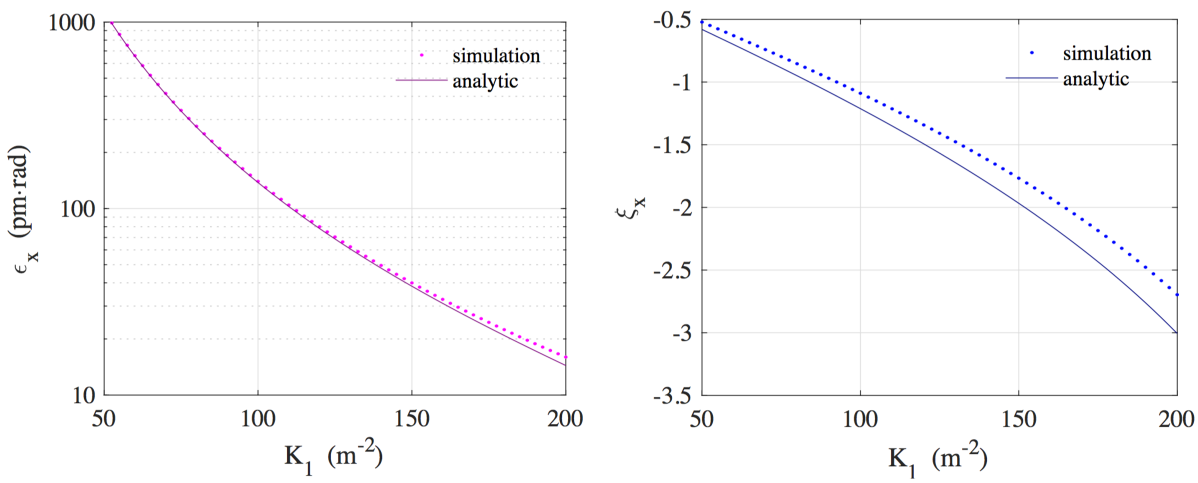

Fig. 5: Scaling of emittance and chromaticity (a single magnet with 10 periods) as a function of the focusing gradient.

From Fig. 5 follows that the emittance is an exponential function of the quadrupole gradient with the same dipole strength. Thus, if the chosen gradient is 500 T/m for a 3 GeV ring then the ring emittance is about 1 nm, which is an order of magnitude higher than for the case of 1000 T/m. Therefore, future R&D on the Complex Bend concept should be focused, as the first step, on demonstrating highest achievable gradients on the scale of a single cell and, then, integration of multiple cells into a single unit. Number of dipole poles and their field also define the ring emittance and are subject for optimization for a given ring lattice.

Chromaticity in the Complex Bend lattice can be estimated as $\xi_x \approx -\frac{L_q N_p}{4\pi}(K_{1F}\beta_{xmin} + K_{1D}\beta_{xmax})$ with L_q is the length of the pole and N_p is number of periods in the unit and similar for ξ_y.

From the second plot in Fig. 5 we conclude that the Combined Bend totals chromaticity of 1.1 per single element, which amounts to the chromaticity of 66 for the ring comprised out of 60 dipoles with the total angle of 2·π. The optics between Complex Bends will need to be designed to amplify dispersion and beta-functions so to minimize the strength of chromatic sextupoles.

3. Complex Bend design considerations and practical limitations

The following figure 6 illustrates the engineering concept behind the Complex Bend. The element consists of short quadrupoles of alternating polarity separated by short dipoles. The element's axis is bent following the small bending angles from the dipole poles.

The distance between consecutive quadrupoles and dipoles should be sufficiently long to minimize areas with combine dipole and quadrupole fields, as well as reducing high multipoles. The former will lead to modification of the ring J_x through I_4 synchrotron integral and may result in partition number J_z becoming negative if not controlled.

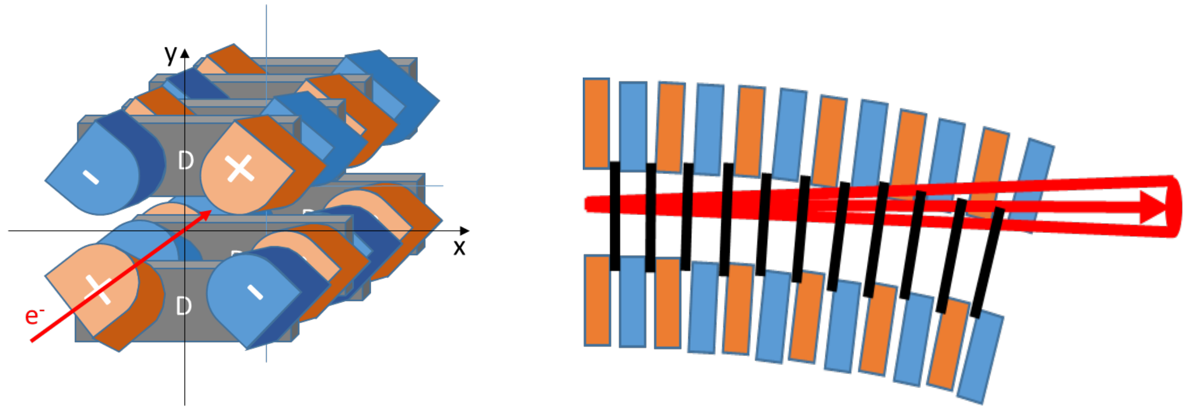

Fig. 6: Cartoons illustrating the concept of Complex Bend. The right cartoon shows top view and radiation cone generated from the entrance of the device.

In Table 2 we calculated parameters of a version of the Complex Bend as installed on NSLS-II storage ring.

Number of poles in the ring	1200	X-shift of orbit per dipole, mm	145
Angle per pole, mrad	5.24	K1, m^{-2}	100
Number of periods	600	Magnetic gradient, T/m	1000
Number of dipoles	60	Bore diameter in quad, m	0.01
Number of periods per BW dipole	10	Field on bore edge, T	5.00
Angle per dipole, rad	0.105	Critical wavelength, A	1.98
Quad Pole length, m	0.06	Photon energy, keV	6.27
Dipole Pole length, m	0.05	SR opening half angle at λ_c, m	1.70E-04
Drift between poles, m	0.01	SR half spot size at λ_c at dipole exit, m	4.43E-04
Period length, m	0.26	Energy loss per revolution, keV	754.05
Dipole length, m	2.60	Circulating current, A	0.50
Energy, GeV	3.00	Radiated power in the ring, kW	377.03
Gamma	5871	Radiated power per dipole, kW	6.28
Magnetic rigidity, T m	10.00		
Magnetic field, T	1.047		
Bending radius, m	9.55		

Table 2: Set of sample parameters of Complex Bend as "installed" at NSLS-II, i.e. every DBA dipole replaced by the Combined Dipole alternative.

Since Complex Bend requires fields in excess of 5 T (Table 2), we expect that superconducting magnets should be used and the problem of extraction of synchrotron radiation from the bent path becomes critical. For the 2.6-meter long Complex Bend the radiation fan crosses the footprint given by the bore with radius of 1 cm over the length of the whole unit. The vacuum chamber geometry should allow for opening space between the quadrupole poles so that the radiation will have an escape path. This is one of the challenges that needs to be addressed in the engineering design of the Complex Bend.

4. Particle tracking assuming realistic field models

While designing the magnetic model we prepared a more elaborated field model depicted in Fig. 7. We have taken a nonlinear ramp down of the dipole and quadrupole fields between the poles.

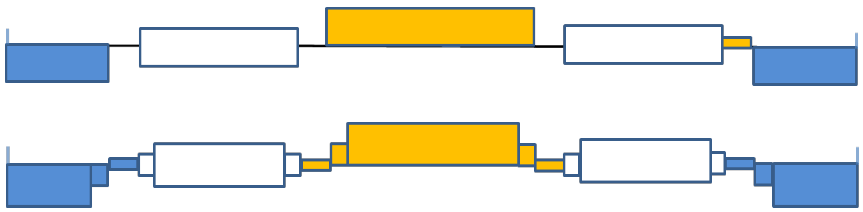

Fig. 7: Complex Bend lattice model that consists of ramp-down fields between the magnet poles.

We assumed in this model that there is an overlap in the drift between two consecutive poles, which contains only both dipole and quadrupole fields. We found that the H-function is a sensitive function of the field fall-off at the magnet edges and are in the process of magnetic design to study the optimal cell geometry minimizing H-function.

At present we are also modelling impact from high order multipoles in between the poles. To minimize this impact we are scanning phase advances with the single cell to approach phases of $n\pi$ (where n is an odd number) between the nonlinear kicks to the particle motion. In contrast to the local compensation of the chromaticity we will manage dispersion and sextupole locations and values in between the Complex Bends in the ring lattice. Managing of nonlinear ring lattice will require clean separation of the dispersive regions of the machine with non-zero bending (localized to within the Complex Bends) and dispersive regions with zero bending, where dispersion will need to be maximized and where the chromatic sextupoles will be located. Orbit through the latter regions will have to be strictly aligned with the multipole centers so to reduce emittance increase due to non-zero magnetic fields on the beam path inside the achromat.

5. Summary

In this paper we compared properties of two lattices, based on DBA and Complex Bend concepts, and found that the latter can lead to substantial (factor of 30) emittance reduction within a certain range of the field properties. As the bending is localized to a relatively short length, the lattice based on Complex Bends may deliver substantial extra space for insertion devices in a synchrotron light source.

We illustrated the benefit of our concept in the next figure (Fig. 8), where we picked several upgrade projects that reach low emittance by replacing their rings with these based on the MBA lattices preserving the same symmetry of the lattice to match the locations of beam lines. As a rule, every project replaces DBA or TBA lattices by going to 7- or 9-BA solutions and gaining a factor of 2-4 in the number of dipoles. Most aggressive path is chosen by MAX-4 upgrade [6] that considers 19-BA lattice, taking over most of the ring circumference by the bending arc elements. By our concept we are able to keep the same number of dipoles in the ring, however, every dipole consists of the 10-20 poles, which enables large factor in reduction of the machine emittance.

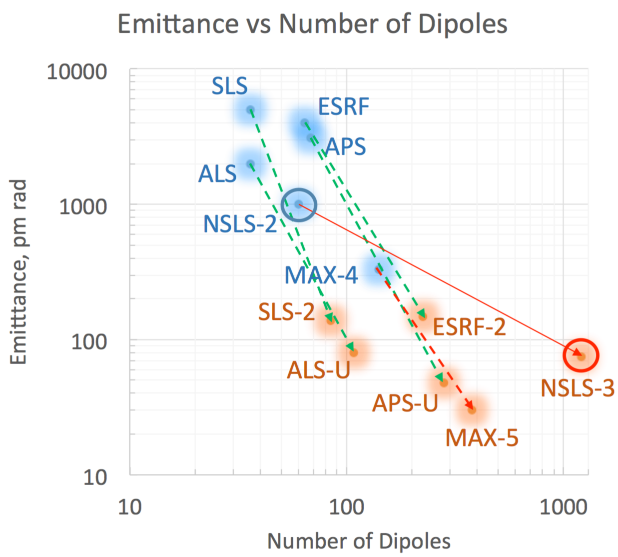

Fig. 8: Illustration of emittance reduction via increasing number of dipoles in the modern MBA upgrade projects. We include the Complex Bend concept applied to NSLS-II as an insightful comparison with the conventional approach.

We are concluding this note with the following few remarks. The FODO like structure is natural for many types of circular machines and high-field magnet lattices were implemented in FFAG lattices in particular. An insightful example of compact and completely superconducting ring lattice is PAMELA, non-scaling FFAG developed in the UK [7]. The field in the main dipoles amounts to 5 T. Our concept of Complex Bend uses a similar approach, however, FODO in the Complex Bend is arranged into a single periodic structure replacing a conventional bending magnet so to minimize the H-function and, therefore, the machine emittance.

On other hand, the periodic sequence of FODO cells reminds of a high-field wiggler. Our choice of 5 T field producing gradients of 1000 T/m was not random. As we at NSLS-II are in the process of constructing High-energy X-ray beamline we will be using a Superconducting Wiggler (SCW) with 4.5 T peak dipole field, vertical aperture of 1 cm and period length of 5 cm [8]. The technological approach in developing compact poles of SCWs with high field exists today and reached high degree of maturity [9].

Superbends (isolated poles with high magnetic field to extend photon spectrum for the user experiments) are easy to realize in Compact Bend structure: one could increase the field of several poles to 5 T taking penalty of somewhat increasing emittance without increasing the device cost.

Speaking of the cost, the Compact Bend is based on superconducting magnet technology and thus is far more complex and expensive as compared with the regular bends. However, it will greatly reduce complexity of power supplies and vacuum chambers as compared with the machine design based on the MBA lattice and lead to very substantial space savings in the ring. Also, superconducting technology in modern light sources is not unusual – LCLS-II Free Electron Laser [10] is based on a hundred of Superconducting RF structures operating at 2K.

Still, reaching such high levels of field gradients needs to be proven feasible. If only a fraction of the required gradient is practical then Complex Bend is just an academic exercise. The next step is to design a magnetic model and build a prototype. During our recent iteration on the Complex Bend lattice we found that the emittance of 68 pm rad is feasible for NSLS-II with longer pole length and gradients about 600 T/m.

This paper is not intended to give an engineering design of the Complex Bend element and the lattice solution for the ring based on this concept. At this point, we are developing magnetic field and Synchrotron Radiation models and discussing general requirements on the beam optics in a storage ring that would employ our concept.

Acknowledgements

T. Shaftan expresses thanks to B. Parker, O. Tchoubar and N. A. Mezentsev for helpful discussions on the magnetic design of the Complex Bend cell.

References

[1] A Lattice Design to Reach the Theoretical Minimum Emittance for a Storage Ring, D. Einfeld, J. Schaper and M. Plesko, http://citeseerx.ist.psu.edu/viewdoc/download?doi=10.1.1.495.2446&rep=rep1&type=pdf

[2] ESRF upgrade phase II status, J-L. Revol et al., Proc. of IPAC-2014, Dresden, Germany, MOPRO055, pp 209-212, http://www.esrf.eu/Apache_files/Upgrade/ESRF-orange-book.pdf

[3] Status of the APS upgrade project, S. Henderson, Proc. of IPAC-2015, Richmond, VA, USA, TUPJE067, pp 1791-1793, http://accelconf.web.cern.ch/AccelConf/IPAC2015/papers/tupje067.pdf

[4] Physics design progress towards a diffraction limited upgrade of the ALS, C. Steier, J. Byrd, H. Nishimura, D. Robin and S. De Santis, Proc. of IPAC-2016, Busan, Korea, WWPOW049, pp 2956-2958, https://indico.cern.ch/event/574973/contributions/2329244/attachments/1362489/2068386/01-ALS-U-Talk-LER2016-David_Robin.pdf

[5] SIRIUS status report, A.R.D. Rodrigues et al., Proc. of IPAC-2016, Busan, Korea, WEPOW001, pp 2811-2814, https://accelconf.web.cern.ch/accelconf/IPAC10/papers/wepea006.pdf

[6] Future development plans for the MAX IV light source: Pushing further towards higher brightness and coherence, P. F. Tavares, J. Bengtsson and Å. Andersson, Journal of Electron Spectroscopy and Related Phenomena, 2017, http://www.sciencedirect.com/science/article/pii/S0368204816302134

[7] PAMELA overview and status, K. Peach et al., Proc. of IPAC-2010, Kyoto, Japan, MOPEA021, pp 112-114, https://accelconf.web.cern.ch/accelconf/pac2009/papers/mo6pfp073.pdf

[8] RSI for the Superconducting Wiggler Source and Front-End for the HEX Beamline, NSLS-II record, PS-C-XFD-RSI-HEX-001, June 2017

[9] Superconducting Wigglers, N. Mezentsev and E. Wallen, Synchrotron Radiation News, Vol. 24, 2011, Issue 3, pp 3-9, https://www.researchgate.net/publication/233221877_Superconducting_Wigglers

[10] LCLS-II: status of the CW X-ray FEL upgrade to the SLAC LCLS facility, T. O. Raubenheimer, Proc. of FEL-2015, Daejeon, Korea, WEP014, pp 618-624, http://accelconf.web.cern.ch/AccelConf/FEL2015/papers/wep014.pdf